Title

Amyloid-β (Aβ42) Peptide Aggregation Rate and Mechanism on Surfaces with Widely Varied Properties: Insights from Brownian Dynamics Simulations

Journal

The Journal of Physical Chemistry B, 124(27)

ISSN

1520-6106

Authors

Cholko, Timothy
Barnum, Joseph
Chang, Chia-en A

Publication Date

2020-07-09

DOI

10.1021/acs.jpcb.0c02926

Peer reviewed

HHS Public Access

Author manuscript

J Phys Chem B. Author manuscript; available in PMC 2021 January 10.

Published in final edited form as:

J Phys Chem B. 2020 July 09; 124(27): 5549–5558. doi:10.1021/acs.jpcb.0c02926.

Amyloid-β (Aβ42) Peptide Aggregation Rate and Mechanism on Surfaces with Widely Varied Properties: Insights from Brownian Dynamics Simulations

Timothy Cholko, **Joseph Barnum**, **Chia-en A. Chang**

Department of Chemistry, University of California, Riverside, Riverside, California 92521, United States;

Abstract

Amyloid-β (Aβ) plaques, which form by aggregation of harmless Aβ peptide monomers into larger fibrils, are characteristic of neurodegenerative disorders such as Alzheimer's disease. Efforts to treat Alzheimer's disease focus on stopping or reversing the aggregation process that leads to fibril formation. However, effective treatments are elusive due to certain unknown aspects of the process. Many hypotheses point to disruption of cell membranes by adsorbed Aβ monomers or oligomers, but how Aβ behaves and aggregates on surfaces of widely varying properties, such as those present in a cell, is unclear. Elucidating the effects of various surfaces on the dynamics of Aβ and the kinetics of the aggregation process from bulk solution to a surface-adsorbed multimer can help identify what drives aggregation, leading to new methods of intervention by inhibitory drugs or other means. In this work, we used all-atom Brownian dynamics simulations to study the association of two distinct Aβ42 monomer conformations with a surface-adsorbed or free-floating Aβ42 dimer. We calculated the association time, surface interaction energy, surface diffusion coefficient, surface residence time, and the mechanism of association on four different surfaces and two different bulk solution scenarios. In the presence of a surface, the majority of monomers underwent a two-dimensional surface-mediated association that depended primarily on an Aβ42 electrostatic interaction with the self-assembled monolayer (SAM) surfaces. Moreover, aggregation could be inhibited greatly by surfaces with high affinity for Aβ42 and heterogeneous charge distribution. Our results can be used to identify new opportunities for disrupting or reversing the Aβ42 aggregation process.

Graphical Abstract

Corresponding Author: Chia-en A. Chang – Department of Chemistry, University of California, Riverside, Riverside, California 92521, United States, chiaenc@ucr.edu.

Supporting Information

The Supporting Information is available free of charge at https://pubs.acs.org/doi/10.1021/acs.jpcb.0c02926.

Table comparing β-sheet and random coil monomer conformation results; computational details for the Brownian dynamics algorithm; additional details regarding the chosen association criteria; discussion of the in-house program used to measure monomer adsorption and desorption; detailed calculations and discussion of theoretical association times and their comparison to simulation (PDF)

The authors declare no competing financial interest.

Complete contact information is available at: https://pubs.acs.org/10.1021/acs.jpcb.0c02926

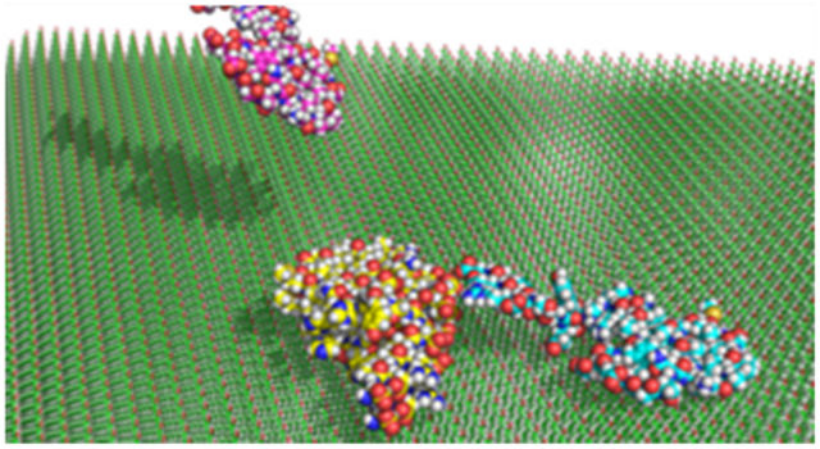

INTRODUCTION

Amyloid-β (Aβ) peptide aggregation has been implicated in the onset and progression of many neurodegenerative disorders including Alzheimer's disease (AD).[1–3] Aβ is a 39- to 42-amino acid intrinsically disordered peptide consisting of a disordered hydrophilic N-terminal tail, a mostly hydrophobic core, and a hydrophobic C-terminus. It has been shown experimentally and computationally that structurally disordered Aβ monomers tend to adopt a more ordered conformation rich in the β-sheet structure after spontaneously associating with another monomer or with a surface.[4,5] These β-sheet-rich structures can then rapidly grow into the larger pathogenic aggregates that are characteristic of AD, known as amyloid plaques.[6–11] Aβ is primarily found in two forms, Aβ40 and Aβ42, depending on the number of amino acids. The latter is the more toxic version, possibly due to its higher β-sheet content, so here we focus solely on Aβ42.[12–14]

Studies *in vitro* and *in vivo* have revealed multiple possible causes of Aβ42 neurotoxicity, many of which involve adsorption of Aβ42 to the cellular surface.[15,16] One such cause is the ability of Aβ42 aggregates to form pore-like structures on cell membranes leading to ion permeability.[17] Two other proposed mechanisms involve the association of Aβ42 with cell membranes, causing thinning and subsequent leakage of small molecules.[18,19] All depend highly on the interaction of Aβ42 with cell membranes, indicating the importance of detailed understanding of the propensity of Aβ42 to adhere to and aggregate on various surfaces as well as the driving forces behind such behavior. Moreover, elucidating the effect of various surfaces on the kinetics and mechanism of monomer association with a preformed fibril may inform new therapeutic methods for inhibiting this process.

Monomers most commonly associate with the fibril through a "dock-lock" mechanism, in which monomers first associate with the fibril surface (dock), and then undergo conformational rearrangement to more strongly associate with the fibril tip (lock).[20–24] Much effort has been spent on stopping or reversing AD progression by inhibiting fibril aggregation with various methods, such as small molecule inhibitors.[25–28] Simulation studies have focused highly on elucidating the dock-lock aggregation mechanism or on the change from a disordered to β-sheet conformation using both all-atom molecular dynamics

(MD)[29–32] and several coarse-grained techniques.[33–35] Other work has investigated the ability of Aβ42 to adsorb to cellular membranes and other material surfaces.[36–39] Aβ42 surface interactions can be modulated by multiple factors such as pH, ionic concentration, surface chemistry, and surface morphology.[40–43] Multiple studies found that Aβ42 primarily adopts a β-sheet-rich conformation upon adsorption to surfaces possessing a wide range of properties.[39,44,45] Moreover, using MD simulations, Thu et al. recently showed that the experimentally measured aggregation rate of Aβ42 is highly correlated with the β-sheet content in the monomeric state.[5]

Many of the detailed computational studies of Aβ have used truncated fragments of the peptide that contain only key residues.[4,46] One shortcoming of this approach is that it excludes charged residues that reside near the N- and C-termini that affect the aggregation of Aβ42. Indeed, a nonzero net charge can cause repulsion between peptides and will affect the interaction with ionic or polar surfaces. There is currently a lack of understanding regarding the aggregation kinetics of Aβ42 peptides in solution and on a surface. Specifically, it is unknown whether aggregation takes place primarily in solution or on surfaces *in vivo* and whether surfaces mediate or inhibit this process. Additionally, cells present chemically diverse structures to diffusing peptides. An understanding of how different environments affect Aβ42 may provide valuable guidance in therapeutic efforts.

Here, we used all-atom Brownian dynamics (BD) simulations to study the association of the Aβ42 monomer with a surface-adsorbed Aβ42 dimer and with a dimer in bulk solvent. In surface-adsorbed dimer scenarios, we used four different self-assembled monolayer (SAM) surfaces of widely varying properties. These simulations replicate the initial stages of Aβ42 fibril aggregation, providing valuable insight into the mechanism and kinetics of the process as it may proceed in a cellular environment. We show that the vast majority of monomers underwent surface-mediated, two-dimensional (2D) association on all surfaces. An inhomogeneous surface strongly inhibited Aβ42 aggregation, and the aggregation rate on all surfaces depended highly on the surface diffusion rate. Additionally, monomers adsorbed and associated with the dimer by a different mechanism depending on surface properties, which may provide insight into theories of Aβ42 neurotoxicity and new methods for inhibiting aggregation.

METHODS

Aβ_{42} Peptide and SAM Structure.

A PDB crystal structure 2NAO, which is a hexamer of Aβ42 in a β-sheet-rich conformation, was modified to obtain an Aβ42 monomer (Figure 1a).[47] For comparison, we also used a random coil conformation of Aβ42 (Figure 1b), which is more commonly observed during free diffusion in solution.[48] This conformation was obtained from an MD simulation of Aβ42 monomers in solution using a specialized force field for disordered peptides.[49] Both conformations have a $-3e$ charge. The monomer was diffused during the simulations until it associated with the surface-adsorbed (Figures 1b and 2a) or free-floating (Figure 2b,c) Aβ42 dimer, which was stationary in all cases. The dimer used in all simulations was also derived from PDB 2NAO, so it too is a β-sheet-rich conformation. More details on the choice of Aβ42 conformation are available in the Supporting Information. The four SAM surfaces

used were undecanethiol (hydrophobic), 11-mercapto-1-undecanol (hydrophilic), 11-amino-1-undecanethiol (cationic), and 11-mercaptoundecanoic acid (anionic) on a gold substrate. We refer to these as the CH_3−, OH−, NH^+−, or COO^--SAM, respectively. All SAMs were constructed according to the lowest-energy conformation of alkanethiol SAMs on Au(111) described by Schreiber.[50] The chains have a hexagonal packing pattern and a packing density in the order of 10^{14} cm^{-2}, yielding an average chain separation of 4.98 Å. The ionizable SAMs (NH^+-SAM and COO^--SAM) were modeled as they would appear at pH 7. For the COO^--SAM, this means that all tail groups were in the deprotonated COO^- form, and for the NH^+-SAM, randomly selected 30% of the tail groups were in the protonated NH_3^+ form, whereas the rest were in the neutral NH_2 form.[51]

Simulation Protocol.

We performed all-atom BD simulations with the GeomBD3 program.[52] The SAMs with an adsorbed Aβ42 dimer were placed at the bottom of a rectangular prism that extended 500 Å in the *z*-dimension and 280 Å in the *x*- and *y*-dimensions (Figure 2a). Hereafter, we refer to the SAM/dimer structure as the “receptor”. Monomers began diffusion from a random position on the *x*-*y* plane at a height of 400 Å above the receptor. The side faces of the prism used periodic boundary conditions and were placed 50 Å before the edges of the SAM to prevent monomers from hanging over the edge or going below the SAM.

Simulations included a stationary grid representation of the receptor’s volume, electric field, and the van der Waals (vdW)-like 12–6 Lennard-Jones (LJ) potential. The grid spacing for all of the three grids was 0.5 Å. The electric field and LJ grids extended 40 Å and 15 Å, respectively, beyond all edges of the receptor. Atomic charges and LJ parameters for Aβ42 were derived from the AMBER ff14SB force field.[53] Atomic charges for the SAM molecules were calculated using the AMBER antechamber program with the AM1-BCC semi-empirical charge method,[54] and LJ parameters were taken from AMBER ff14SB. During simulation, monomers diffuse in implicit water solvent according to the overdamped Langevin equation

$$r_i(t+\Delta t) = r_i(t) - \frac{D_i}{k_B T}\frac{dU}{dr} + \sqrt{2D_i\Delta t}R \quad (1)$$

where D_i is the translational or rotational diffusion coefficient, k_B is Boltzmann’s constant, T is the temperature (298.15 K), $\frac{dU}{dr}$ is the potential energy gradient, Δt is the time step, and R is a zero-mean stationary Gaussian process.[55] If monomers diffused past the top of the simulation box, they were returned to their previous position and a new diffusion step was calculated with a different random force. Translational and rotational diffusion coefficients were calculated from the Stokes-Einstein equation. Additional details are available in the Supporting Information. For computational efficiency, a distance-dependent variable time step between 0.1 and 1.0 ps was used. The time step was scaled linearly between these two values based on the distance between the centers of the monomer and dimer, taking on larger values with increasing distance. Below a distance of 50 Å, the time step was always 0.1, and above 500 Å it was always 1.0 ps.

Calculation of Self-Diffusion Coefficients.

Bulk and surface self-diffusion coefficients, D and D_{surf}, respectively, of Aβ42 were calculated by the Einstein relation $\left\langle r^2 \right\rangle = \lim_{t \to \infty} 2nDt$, where r is the displacement in time t, D is the diffusion coefficient, and n is the dimensionality of the diffusion process on sections of monomer trajectories of at least 500 ns.

Aβ42 Association Mechanism and Surface Residence Time.

Because these simulations used rigid molecules with no internal degrees of freedom, it was necessary to define a coarse geometric "association criterion", which, once satisfied, records the trajectory as an association event. Our association criterion requires the distance between the phenylalanine residues buried in the hydrophobic core region of a monomer and the surface-adsorbed dimer to come within 40 Å of each other (Figure 3). Additional details can be found in the Supporting Information. The association mechanism was analyzed for each monomer-dimer association event and was classified as either 2D or three-dimensional (3D) associator. 2D associators are monomers that satisfied the association criterion while simultaneously being adsorbed to (or just after desorption from) the surface. 3D associators are monomers that satisfied the association criterion while diffusing in the bulk solvent, regardless of whether they had adsorbed to the surface earlier in their trajectory. Surface residence time is defined as the average time a monomer stayed adsorbed to a SAM before desorbing or associating with the dimer. More details are available in the Supporting Information.

Kinetic Theory of Molecular Association with Surface-Bound Receptors.

We compared the simulation data to the 2D and 3D association rate theory. Theoretical 3D and 2D average association times, τ_3 and τ_2, respectively, depend highly on the radius of the final target a (the dimer) and radius of the search space b (the simulation box or SAM) as well as the bulk or surface diffusion rate D or D_{surf}

$$\tau_3 = \left(\frac{b^2}{D}\right)\left(\frac{1 - \left(\frac{a}{b}\right)^2}{3\frac{a}{b}}\right) \tag{2}$$

$$\tau_2 = \left(\frac{b^2}{D_{surf}}\right)\left(\frac{1}{1.103^2}\right) \tag{3}$$

In this work, the overall theoretical average association time, t_{theo}, for a 3D associating monomer is $\tau_{3,\,dimer}$, where the subscript dimer indicates the final target. For a 2D associating monomer, t_{theo} is $\tau_{3,\,SAM} + \tau_2$ because it must first diffuse three-dimensionally to the SAM from its starting position then two-dimensionally to the dimer.[56,57] Since there is no derivation of a theoretical average association time that clearly corresponds to diffusion from the starting plane to the SAM, we instead used a time derived from the simulations having no-surface, in which the dimer was at the bottom of the box. The radius of the dimer is more than 3 times smaller than the SAM, so the time to reach a SAM of the same distance

from the starting plane will be significantly lower. We assume that this time $\tau_{3,\ \mathrm{SAM}}$ is 3 μs, roughly half that to reach the dimer (Table 1). The increase in the association rate due to reduction of dimensionality can be large, assuming that $b \gg a$ and that D and D_{surf} are similar, but this is not always the case for a charged peptide on certain surfaces. Here, we used a = 40 Å for the dimer and b = 140 Å for both the simulation box and the SAM. We note that eqs 2 and eqs 2 are most accurate when $a/b \leq 0.1$ (i.e., the search space is at least 10 times larger than the final target), in which case the factor 1.103 is used in eq 3.[57] To calculate t_{theo} for the ensemble of more than 1000 associated trajectories in each scenario, we weight the 2D and 3D theoretical average association times by the percentage of trajectories that are associated with each mechanism

$$t_{\mathrm{theo}} = m^{*}\left(\tau_2 + \tau_{3,\ \mathrm{SAM}}\right) + n^{*}\tau_{3,\ \mathrm{dimer}} \tag{4}$$

where m and n are the percentages of 2D and 3D associating trajectories, respectively. More detailed calculations can be found in the Supporting Information.

RESULTS AND DISCUSSION

Assembly of Aβ peptides into toxic fibrils may be affected by the presence of a surface and the surface's chemical properties. Wang et al. previously found that surfaces can accelerate the formation of fibrils by mediating important interactions that induce a conformation favorable to fibrillization.[39] However, He et al. recently found that an inhomogeneous graphene oxide surface severely disrupted the aggregated fibril structure.[42] To investigate surface effects, we used BD simulations to study diffusion of an Aβ42 monomer to a surface-adsorbed or free-floating Aβ42 dimer. Because we used rigid-body molecular models that exclude internal degrees of freedom, we focused only on the process of monomer diffusion to the dimer such that the binding criterion is satisfied. This process still allows for elucidating the effects of different surfaces on initial stages of fibrillization.

The surfaces were SAMs of functionalized alkanethiols chosen to have hydrophilic, hydrophobic, cationic, or anionic properties. For comparison, two simulations were run with no-surface present, in which the Aβ42 dimer was located at the bottom (Figure 2b) or in the center (Figure 2c) of the simulation box. To ensure convergence of the calculated properties, we ran the simulations until at least 1000 trajectories achieved association. We focused on elucidating several phenomena: Aβ42 adsorption and diffusion on each surface, the mechanism of monomer-dimer association on each surface, and the average association time in each case. We also compared the simulation results to theoretical monomer-dimer association times and found that our simulations generally yielded faster association, which is discussed in the following sections. Still, the simulation results can be usefully compared to theory to elucidate surface effects on Aβ42 association and assess the applicability of the theory in various scenarios.

AB_{42} Surface Interactions and Association Rate.

CH_3-SAM.—The undecanethiol SAM presents a hydrophobic surface to the diffusing Aβ42 monomer. On this surface, we simulated β-sheet and random coil monomer conformations. The adsorption orientation of the β-sheet (Figure 4a) and random coil maximized monomer-

SAM intermolecular contacts. Surface interaction energy analysis showed strong vdW attractions as the driving force behind adsorption to the surface and very little electrostatic attraction (Table 1). Notably, the coil experiences far weaker vdW attraction, which is likely the reason for its much faster surface diffusion. Wang et al. showed experimentally that Aβ42 adsorbed readily to a CH_3-SAM, even more than to a hydrophilic or an anionic surface.[4] The energy landscape as the peptide diffuses across the nonpolar surface is smooth, yielding a relatively high diffusion rate for the β-sheet and coil, 8.76×10^{-8} cm^2 s^{-1} (Table 1) and 17.5×10^{-8} cm^2 s^{-1}, respectively. The average monomer-dimer association time, t_{avg}, for the β-sheet was the second fastest among all six surfaces tested, at 9.08 μs. This is likely the result of fast surface diffusion and isotropic affinity of Aβ42 for this SAM. The coil showed a t_{avg} of 5.42 μs. The faster association of the coil is proportional to its higher surface diffusion coefficient; both properties differ between conformations by a factor of approximately 2. Typically, monomers must be able to rotate or partially desorb from the SAM to meet the association criterion. Hence, a high association rate requires efficiently diffusing to the dimer and then overcoming the energy barrier of reorientation to bind. We found, in general, a direct relationship between the surface diffusion coefficient D_{surf} and t_{avg} (Figure 5). Our calculated 2D:3D binding ratios of 8.9 and 7.6 for the β-sheet and coil, respectively, indicate that approximately 90% of the association on this SAM was surface-mediated for both conformations, hence the strong dependence on D_{surf}. Aβ42 monomers approaching the receptor tended to adsorb steadily to the SAM, then diffuse two-dimensionally before associating with the dimer. This resulted in the highest average surface residence time measured, 7.88 μs (Table 1).

OH-SAM.—The 11-mercapto-1-undecanol surface is hydrophilic, but the dynamics of Aβ42 on the surface was in many ways very similar to the CH_3-SAM. D_{surf} was 7.36×10^{-8} cm^2 s^{-1} (Table 1), which is only marginally slower than on the hydrophobic surface. Again, the driving force of adsorption was vdW attraction (Table 1), with the monomers lying in the same flat orientation (Figure 4b). However, in contrast to the hydrophobic SAM, a significant amount of 3D association occurred on this surface, for a 2D:3D ratio of just 2.7 (Table 1). Of note, this SAM was the only one showing a repulsive term in the energy analysis, for a mean E_{elec} of 0.311 kcal mol^{-1}. The lack of long-range attractive electrostatic forces to the SAM gives monomers a greater chance to remain in solution and associate three-dimensionally. This observation exemplifies a general trend in our findings that points to electrostatic attractions as the primary determinant of the association mechanism, with less attraction leading to greater amount of 3D association. Monomers that adsorbed resided on the surface for 6.82 μs on an average before associating or desorbing, indicating that adsorption was maintained once the highly attractive vdW forces were formed. Here, t_{avg} was 10.31 μs (Table 1), slightly slower than on the CH3-SAM, in keeping with the positive trend between $1/t_{avg}$ and D_{surf}.

NH^+-SAM.—As on the CH_3-SAM, we simulated β-sheet and coiled Aβ42 conformations for comparison on this surface. The plot of electrostatic and vdW interaction energy on the NH^+-SAM unsurprisingly shows a highly attractive electrostatic potential between both monomer conformations and the SAM, due to the $-3e$ net charge on the monomer and $+1e$ net charge on the NH_3^+ tail groups. This surface was modeled with a randomly selected 30%

of the SAM tail groups in the protonated NH_3^+ form to mimic the surface at a pH of 7, whereas the rest of the tail groups were NH_2. As a result, the inhomogeneous distribution of positive charge tended to constrain the monomers to certain positions on the SAM where the charge density was highest (Figure 4c). This phenomenon, which was observed for both β-sheet and coil conformations, was so strong that it held the Aβ42 monomers practically immobile, rendering measurement of an accurate diffusion coefficient impossible in the time scales accessible by the simulation. Attraction to the surface was so great that only a small handful of monomer trajectories ever associated with the dimer after several thousand CPU-hours of simulation. Monomers were incapable of diffusing toward the dimer and reorienting to satisfy the association criterion. This result again agrees with our observed relationship between D_{surf} and t_{avg}. In this case, it represents an extreme example in which these properties were too slow to be measured computationally. He et al. observed a similar behavior of Aβ in their MD simulations of Aβ on an inhomogeneous graphene oxide surface, during which Aβ monomers preferentially remained disassociated from each other and adsorbed strongly to highly polarized portions of the graphene oxide surface.[42] Our NH-SAM results demonstrate that a highly inhomogeneous charge distribution can severely disrupt Aβ42 aggregation on a surface regardless of the conformation by sequestering Aβ42 to areas of the surface with high affinity. To represent conditions that may be more similar to those that may be encountered *in vivo* or *in vitro*, we repeated these simulations on an NH^+-SAM with adsorbed Cl^- counterions, which we refer to as the NH^+-SAM(i). These results are discussed in a section later (Table 2).

COO^--SAM.—Aβ42 dynamics on this surface was driven by electrostatic attractions of the cationic amino acid residues with the anionic COO^- tail groups. We observed a unique adsorption orientation in which monomers orient the positively charged residues to the surface (Figure 4d). Despite the $-3e$ overall charge per monomer, the monomers achieved a net electrostatic attraction in this orientation (Table 1). The total E_{surf} was higher than with the other SAMs, primarily because of less intermolecular contacts yielding far less vdW attraction. This finding could explain the t_{res} on this SAM, 6.35 μs, which was the lowest calculated. Aβ42 tended to experience brief desorption quickly followed by re-adsorption. Still, the 2D association mechanism was by far the dominant one, indicating that the monomers tended to be corralled in by the surface and remained in the vicinity rather than diffusing back into the bulk solvent where they have a chance to associate three-dimensionally. Despite high electrostatic attractions, D_{surf} was 7.50×10^{-8} cm^2 s^{-1} (Table 1), nearly matching that on a nonpolar SAM, because the distribution of negative charge is isotropic. This yielded a t_{avg} of 10.01 μs. The main difference between this surface and the OH-SAM was the electrostatic repulsion of monomers from the latter, resulting in a significantly higher fraction of 3D association in that case. Here 2D:3D was 13.5, the highest measured (Table 1). The agreement with the theoretical association time here was similar to that on the other surfaces, for t_{theo}/t_{avg} = 2.38 (Table 3).

Inclusion of Explicit Ions on Formally Charged SAMs.

We performed identical simulations for the formally charged SAMs with and without explicit monovalent counterions adsorbed to the surface. We indicate the SAMs with explicit counterions by an (i) next to the name. The conformation of ions adsorbed to the SAMs was

determined from MD simulations of each SAM in explicit water and 0.1 M NaCl. From these simulations, we calculated the position and surface density of adsorbed counterions and built model SAMs for BD simulation with the same properties. On the NH^+-SAM(i), adsorbed Cl^- ions altered the monomer-SAM interactions sufficiently so that Aβ42 diffused two-dimensionally. Under these conditions, the diffusion coefficient was 6.18×10^{-8} cm^2 s^{-1} (Table 2), a marked increase from the practical immobility of monomers when counterions were absent. However, the areas of highest positive charge density still tended to immobilize some of the diffusing monomers, similar to the case on this surface without ions. When monomers diffused to these spots, they tended to remain there for the duration of the simulation. As a result, we were unable to sample a sufficient number of associating trajectories to calculate accurate values of t_{res} and t_{avg}, and the calculated D_{surf} should be thought of as an upper limit of the value.

On the COO^--SAM(i) with explicit surface-adsorbed Na^+ ions, the average association time decreased to 8.01 μs as compared with the 10.0 μs without counterions (Table 2). The ions lowered the affinity of Aβ42 to the SAM and more than doubled D_{surf} to 15.6×10^{-8} cm^2 s^{-1} (Table 2). This was easily the highest diffusion rate on any SAM and yielded the fastest t_{avg} for any surface. Average surface residence time was reduced substantially to 3.62 μs after the addition of the ions. However, this was in part due to the faster surface diffusion and thus faster association and not only due to monomers desorbing more quickly from the SAM. Additionally, 2D:3D was lowered from 13.5 to 4.68 (Tables 1 and 2), thereby indicating a shift of the association mechanism toward a greater fraction of 3D association. We found the closest agreement with theoretical association time on this surface since the high D_{surf} yielded a lower theoretical time more in line with the simulation (Table 3). Results from both explicit counterion simulations illustrate the importance of ionic concentration and ion adsorption to charged surfaces when interpreting or predicting the Aβ behavior at a surface or other interface. The most strongly impacted parameter was D_{surf}, owing to the tendency of counterions to mitigate charge anisotropy on a surface, which was the foremost impediment to rapid diffusion. Moreover, as compared with the other properties measured, D_{surf} was correlated most highly with t_{avg} (Figure 5), which further highlights the key role of ions at charged interfaces.

Aβ_{42} Association in Bulk Solution.

The affinity of Aβ42 for the SAMs greatly hindered its ability to search two-dimensionally for the dimer but simultaneously reduced the space that must be searched by anchoring the monomers to the lower-dimensional structure (SAM) containing the final target (dimer). The monomer diffusion coefficient in bulk water, D, was very close to that on most SAMs, at 7.95×10^{-8} cm^2 s^{-1} (Table 2). When the dimer was placed at the bottom of the box in the absence of a surface, t_{avg} was 6.09 μs (Table 2). In this case, the dimer is only accessible from one side; however, there is no SAM present to interact with Aβ42 and subsequently, no anchoring of Aβ42 to a 2D structure. This setup allows us to study the effects of reduction of dimensionality and intermolecular forces on association kinetics. However, the no-surface scenarios diffuse the monomer using the relative diffusion coefficient in eq 1, that is, the diffusion coefficient of the monomer plus that of the dimer, to emulate a real bulk solution environment in which both bodies would be diffusing. This increases the monomer diffusion

rate by a factor of ~1.78 relative to the surface-containing simulations, which employ the self-diffusion coefficient of the monomer. To make a useful comparison of surface and no-surface association times, we can compensate for the difference in the monomer diffusion rate to isolate the effects of the system geometry and monomer-SAM intermolecular forces. We would expect to see an association time ~6.09 × 1.78 = 10.8 μs for the no-surface (bottom) scenario if the self-diffusion coefficient was used, that is, if monomers diffused at the same rate as the surface-containing simulations. This indicates a 5–35% decrease in association time due to the presence of a surface (Tables 1 and 2), which is in good agreement with existing work that suggests that the fibrillization phenomenon may be expedited by surfaces of a wide range of properties.[58,59] For this scenario, $t_{theo} = \tau_3 = 8.26$ μs (Table 3), predicting an approximately 36% higher association time than the simulations.

When the dimer was positioned in the middle of the simulation box (Figure 2c), the association was considerably faster, about double of that in the bottom position. In the middle of the box, the dimer was accessible from both sides, which approximately doubles its effective capture radius of incoming monomers. Once again, $t_{theo} = 8.26$ μs for this case because changing the dimer position does not affect the theoretical rate. However, our simulation results gave $t_{avg} = 3.34$ μs (Table 2). Possible reasons for disagreement between the simulated and theoretical rate are discussed in the following section.

Comparison of Simulation Results and Theoretical Association Times.

Comparing our simulated association time t_{avg} with theoretical values t_{theo} provides ideas to further develop theories describing molecular association in a cell-like environment, where binding usually occurs in a crowded environment with nonspecific attractions.[60] In this study, the major reason for the discrepancy was that the theoretical rates were most accurate when $a/b \leq 0.10$, where a and b are two spheres or circles.[57] In our simulations, $\frac{a}{b} = \frac{40}{140} = \sim 0.29$, which can lead to overestimation of association times. The agreement was better when the dimer was in the bottom position, likely because it was simply further from the starting plane than when positioned in the center. Theoretical times are derived as averages over all possible starting positions, so starting all trajectories from a single plane complicates comparisons. Another possible reason for the discrepancy between simulation and theory is the exclusion of influence due to intermolecular potential in the theoretical rates.

To test the effect of intermolecular potentials on t_{avg}, we repeated simulations of the no-surface scenario, in which the dimer was at the center of the simulation box with the electrostatic and LJ potential grids turned off (i.e., no interaction at all between the monomer and dimer). In this scenario, t_{avg} increased from 3.34 to 3.54 μs. This slight increase indicates weak attractive potential between the monomer and dimer that sped up the association. The reason that association time appears to be only slightly reduced by this intermolecular attraction is likely due to the monomer and dimer both having a net negative charge. As a result, long-range electrostatic steering to accelerate molecular association is unlikely. However, because of large separation of the positively and negatively charged residues on the peptides, attractive forces can be achieved when the two molecules encounter each other, thereby resulting in a slightly faster association. The use of a stationary dimer in

the surface-adsorbed dimer scenarios could have slowed association. However, we are implying here a situation where there is a preformed fibril on a surface that is either stationary or diffuses slowly compared to the monomer, so its diffusion should have a negligible effect on the overall association rate. Even though we used a surface-adsorbed dimer, we can generalize our results to larger fibrils, which would diffuse even more slowly relative to the monomer. In the no-surface scenarios, our simulations used the monomer-dimer relative diffusion coefficient to calculate monomer trajectories, which accounts for the fact that the dimer, too, would be diffusing in a real situation.

In general, because the ratio a/b was relatively large as compared with the assumptions of the theory, simulation matched theory more closely when the dimer was at the bottom of the simulation box—whether it was surface-adsorbed or not—than when it was in the middle. Two factors may contribute to this result. One is that the dimer is simply further away from the starting plane, so there is less overestimation of association times by the theory, and the second is that the surfaces yield a very high proportion of 2D association, for which the theoretical rate depends much less on a/b.[56] The overall association time was dominated by the 2D search, as evidenced by t_{res}, the average time monomers resided on the surface before associating or desorbing, being only slightly lower than t_{avg} in most cases. For example, on the OH-SAM, t_{res} = 7.88 μs and t_{avg} = 9.08 μs (Table 1), meaning the entire lifetime of the average trajectory was only about 1 μs longer than the time it spent on the SAM. Moreover, monomer-SAM intermolecular potential (as opposed to the weak monomer-dimer attraction) is probably dominant and is, to a large extent, accounted for in the surface diffusion coefficient D_{surf}. Thus, the comparison of these results to theory, which ignores intermolecular potential, may not produce large errors.

CONCLUSIONS

Association of an Aβ42 monomer to an Aβ42 dimer was significantly altered by the presence of a surface and the surface's properties. All four SAM surfaces we tested induced the majority of association to occur two-dimensionally, through a surface-mediated mechanism, which tended to expedite association by roughly 5–35% as compared to simulations with the dimer in bulk solution. The exact ratio of 2D to 3D association depended primarily on the electrostatic interactions between the monomer and SAM, with the OH-SAM yielding the lowest ratio, 2.7, and the COO^--SAM the highest, 13.5. Knowledge of the association pathway is valuable for both understanding and combating Aβ peptide aggregation, as surfaces have a strong influence on the Aβ conformation, and therefore may also affect the effectiveness of potential aggregation-inhibiting drug compounds. Overall, the association time had a more direct relationship with the surface diffusion coefficient than any other single parameter. We also showed that the overall association time was slowed significantly by surfaces with high affinity for Aβ42 and by inhomogeneous surfaces, which present a highly anisotropic 2D diffusion landscape. The monomer conformation primarily influences the surface diffusion rate, which is very strongly correlated with the association time. Although water molecules may affect conformations of disordered proteins,[31,61,62] interactions with the surface are likely more influential on conformation than water. However, the monomer conformation did not affect

the association mechanism significantly and did not alter the observed behavior of adsorbed monomers on a hydrophilic or cationic surface.

Notably, the dynamics on ionized surfaces were greatly affected by the inclusion of explicit surface-adsorbed counterions. Cl^- ions on the cationic NH^+-SAM yielded a monomer surface diffusion rate in the same ballpark as the hydrophilic and hydrophobic SAMs, whereas monomers were practically immobile without counterions. Na^+ ions greatly increased diffusion speed on the COO^--SAM and altered the dominant association pathway. This finding highlights the importance of considering the role of ions *in vitro* and, perhaps more importantly, *in vivo*, where the species and concentration of ions may vary considerably throughout the cell. Moreover, the SAMs we tested presented a very wide range of surface properties, mimicking the diversity of structures present in cellular environments. The comparisons between simulated and theoretical association time also provide ideas for developing theoretical equations for approximating molecular association in a crowded cell-like environment.

Supplementary Material

Refer to Web version on PubMed Central for supplementary material.

ACKNOWLEDGMENTS

This study was supported by the US National Institutes of Health (GM-109045), the US National Science Foundation (MCB-1932984), and the NSF national supercomputer centers (TG-CHE130009). We thank Dr. Joachim Dzubiella for the discussion related to molecular diffusion and associations.

■ REFERENCES

(1). Goedert M; Spillantini MG A century of Alzheimer's disease. Science 2006, 314, 777–781. [PubMed: 17082447]

(2). Koo E; Lansbury P; Kelly J Amyloid diseases: Abnormal protein aggregation in neurodegeneration. Proc. Natl. Acad. Sci. U.S.A 1999, 96, 9989–9990. [PubMed: 10468546]

(3). Knowles T; Vendruscolo M; Dobson C The amyloid state and its association with protein misfolding diseases. Nat. Rev. Mol. Cell Biol 2014, 15, 384–396. [PubMed: 24854788]

(4). Wang Q; Shah N; Zhao J; Wang C; Zhao C; Liu L; Li L; Zhou F; Zheng J Structural, morphological, and kinetic studies of beta-amyloid peptide aggregation on self-assembled monolayers. Phys. Chem. Chem. Phys 2011, 13, 15200–15210. [PubMed: 21769359]

(5). Thu T; Co N; Tu L; Li M Aggregation rate of amyloid beta peptide is controlled by beta-content in monomeric state. J. Chem. Phys 2019, 150, No. 225101. [PubMed: 31202253]

(6). Nguyen PH; Li MS; Stock G; Straub JE; Thirumalai D Monomer adds to preformed structured oligomers of Aβ-peptides by a two-stage dock-lock mechanism. Proc. Natl. Acad. Sci. U.S.A 2007, 104, 111–116. [PubMed: 17190811]

(7). Lomakin A; Teplow D; Kirschner D; Benedek G Kinetic theory of fibrillogenesis of amyloid beta-protein. Proc. Natl. Acad. Sci. U.S.A 1997, 94, 7942–7947. [PubMed: 9223292]

(8). Hellstrand E; Boland B; Walsh D; Linse S Amyloid beta-Protein Aggregation Produces Highly Reproducible Kinetic Data and Occurs by a Two-Phase Process. ACS Chem. Neurosci 2010, 1, 13–18. [PubMed: 22778803]

(9). Cleary JP; Walsh DM; Hofmeister JJ; Shankar GM; Kuskowski MA; Selkoe DJ; Ashe KH Natural oligomers of the amyloid-β protein specifically disrupt cognitive function. Nat. Neurosci 2005, 8, 79. [PubMed: 15608634]

(10). Shankar GM; Bloodgood BL; Townsend M; Walsh DM; Selkoe DJ; Sabatini BL Natural oligomers of the Alzheimer amyloid-β protein induce reversible synapse loss by modulating an NMDA-type glutamate receptor-dependent signaling pathway. J. Neurosci 2007, 27, 2866–2875. [PubMed: 17360908]

(11). Šarić A; Chebaro Y; Knowles T; Frenkel D Crucial role of nonspecific interactions in amyloid nucleation. Proc. Natl. Acad. Sci. U.S.A 2014, 111, 17869–17874. [PubMed: 25453085]

(12). Dahlgren KN; Manelli AM; Stine WB; Baker LK; Krafft GA; LaDu MJ Oligomeric and fibrillar species of amyloid-β peptides differentially affect neuronal viability. J. Biol. Chem 2002, 277, 32046–32053. [PubMed: 12058030]

(13). Small DH; McLean CA Alzheimer's disease and the amyloid β protein: what is the role of amyloid? J. Neurochem 1999, 73, 443–449. [PubMed: 10428038]

(14). Selkoe D; Hardy J The amyloid hypothesis of Alzheimer's disease at 25years. EMBO Mol. Med 2016, 8, 595–608. [PubMed: 27025652]

(15). Friedman R; Pellarin R; Caflisch A Amyloid Aggregation on Lipid Bilayers and Its Impact on Membrane Permeability. J. Mol. Biol 2009, 387, 407–415. [PubMed: 19133272]

(16). Dong XW; Sun YX; Wei GH; Nussinov R; Ma BY Binding of protofibrillar A beta trimers to lipid bilayer surface enhances A beta structural stability and causes membrane thinning. Phys. Chem. Chem. Phys 2017, 19, 27556–27569. [PubMed: 28979963]

(17). Press-Sandler O; Miller Y Molecular mechanisms of membrane-associated amyloid aggregation: Computational perspective and challenges. Biochim. Biophys. Acta, Biomembr 2018, 1860, 1889–1905. [PubMed: 29555191]

(18). Sokolov Y; Kayed R; Kozak A; Edmonds B; McIntire T; Milton S; Cahalan M; Glabe C; Hall J Soluble amyloid oligomers increase lipid bilayer conductance by increasing the dielectric constant of the hydrocarbon core. Biophys. J 2004, 86, 382A.

(19). Butterfield S; Lashuel H Amyloidogenic Protein Membrane Interactions: Mechanistic Insight from Model Systems. Angew. Chem., Int. Ed 2010, 49, 5628–5654.

(20). Esler WP; Stimson ER; Jennings JM; Vinters HV; Ghilardi JR; Lee JP; Mantyh PW; Maggio JE Alzheimer's disease amyloid propagation by a template-dependent dock-lock mechanism. Biochemistry 2000, 39, 6288–6295. [PubMed: 10828941]

(21). O'brien EP; Okamoto Y; Straub JE; Brooks BR; Thirumalai D Thermodynamic Perspective on the Dock- Lock Growth Mechanism of Amyloid Fibrils. J. Phys. Chem. B 2009, 113, 14421–14430. [PubMed: 19813700]

(22). Han W; Schulten K Fibril elongation by Aβ17–42: Kinetic network analysis of hybrid-resolution molecular dynamics simulations. J. Am. Chem. Soc 2014, 136, 12450–12460. [PubMed: 25134066]

(23). Straub JE; Thirumalai D Toward a molecular theory of early and late events in monomer to amyloid fibril formation. Annu. Rev. Phys. Chem 2011, 62, 437–463. [PubMed: 21219143]

(24). Linse S Mechanism of amyloid protein aggregation and the role of inhibitors. Pure Appl. Chem 2019, 91, 211–229.

(25). Hamley I The Amyloid Beta Peptide: A Chemist's Perspective. Role in Alzheimer's and Fibrillization. Chem. Rev 2012, 112, 5147–5192. [PubMed: 22813427]

(26). Zou Y; Qian Z; Chen Y; Qian H; Wei G; Zhang Q Norepinephrine Inhibits Alzheimer's Amyloid-beta Peptide Aggregation and Destabilizes Amyloid-beta Protofibrils: A Molecular Dynamics Simulation Study. ACS Chem. Neurosci 2019, 10, 1585–1594. [PubMed: 30605312]

(27). Kayed R; Head E; Sarsoza F; Saing T; Cotman C; Necula M; Margol L; Wu J; Breydo L; Thompson J; Rasool S; Gurlo T; Butler P; Glabe C Fibril specific, conformation dependent antibodies recognize a generic epitope common to amyloid fibrils and fibrillar oligomers that is absent in prefibrillar oligomers. Mol. Neurodegener 2007, 2, No. 18. [PubMed: 17897471]

(28). Necula M; Breydo L; Milton S; Kayed R; van der Veer W; Tone P; Glabe C Methylene blue inhibits amyloid A beta oligomerization by promoting fibrillization. Biochemistry 2007, 46, 8850–8860. [PubMed: 17595112]

(29). Bellaiche M; Best R Molecular Determinants of A beta(42) Adsorption to Amyloid Fibril Surfaces. J. Phys. Chem. Lett 2018, 9, 6437–6443. [PubMed: 30371082]

(30). Schwierz N; Frost C; Geissler P; Zacharias M From A beta Filament to Fibril: Molecular Mechanism of Surface-Activated Secondary Nucleation from All-Atom MD Simulations. J. Phys. Chem. B 2017, 121, 671–682. [PubMed: 27992231]

(31). Sgourakis N; Yan Y; McCallum S; Wang C; Garcia A The Alzheimer's peptides A beta 40 and 42 adopt distinct conformations in water: A combined MD/NMR study. J. Mol. Biol 2007, 368, 1448–1457. [PubMed: 17397862]

(32). Rosenman D; Wang C; Garcia A Characterization of A beta Monomers through the Convergence of Ensemble Properties among Simulations with Multiple Force Fields. J. Phys. Chem. B 2016, 120, 259–277. [PubMed: 26562747]

(33). Pellarin R; Caflisch A Interpreting the aggregation kinetics of amyloid peptides. J. Mol. Biol 2006, 360, 882–892. [PubMed: 16797587]

(34). Barz B; Urbanc B Minimal Model of Self-Assembly: Emergence of Diversity and Complexity. J. Phys. Chem. B 2014, 118, 3761–3770. [PubMed: 24571643]

(35). Ilie I; den Otter W; Briels W A coarse grained protein model with internal degrees of freedom. Application to alpha-synuclein aggregation. J. Chem. Phys 2016, 144, No. 085103. [PubMed: 26931727]

(36). Yang Z; Ge C; Liu J; Chong Y; Gu Z; Jimenez-Cruz C; Chai Z; Zhou R Destruction of amyloid fibrils by graphene through penetration and extraction of peptides. Nanoscale 2015, 7, 18725–18737. [PubMed: 26503908]

(37). Li C; Mezzenga R The interplay between carbon nanomaterials and amyloid fibrils in bio-nanotechnology. Nanoscale 2013, 5, 6207–6218. [PubMed: 23744243]

(38). Bokvist M; Lindstrom F; Watts A; Grobner G Two types of Alzheimer's beta-amyloid (1–40) peptide membrane interactions: Aggregation preventing transmembrane anchoring Versus accelerated surface fibril formation. J. Mol. Biol 2004, 335, 1039–1049. [PubMed: 14698298]

(39). Wang Q; Zhao J; Yu X; Zhao C; Li L; Zheng J Alzheimer A beta(1–42) Monomer Adsorbed on the Self-Assembled Monolayers. Langmuir 2010, 26, 12722–12732. [PubMed: 20597530]

(40). Lin M; Chen L; Tsai H; Wang S; Chang Y; Higuchi A; Chen W Investigation of the mechanism of beta-amyloid fibril formation by kinetic and thermodynamic analyses. Langmuir 2008, 24, 5802–5808. [PubMed: 18452319]

(41). Moore K; Pate K; Soto-Ortega D; Lohse S; van der Munnik N; Lim M; Jackson K; Lyles V; Jones L; Glassgow N; Napumecheno V; Mobley S; Uline M; Mahtab R; Murphy C; Moss M Influence of gold nanoparticle surface chemistry and diameter upon Alzheimer's disease amyloid-beta protein aggregation. J. Biol. Eng 2017, 11, No. 146.

(42). He Z; Li J; Chen S; Zhou R Surface Inhomogeneity of Graphene Oxide Influences Dissociation of A beta(16–21) Peptide Assembly. J. Phys. Chem. B 2019, 123, 9098–9103. [PubMed: 31566974]

(43). Buell A; Galvagnion C; Gaspar R; Sparr E; Vendruscolo M; Knowles T; Linse S; Dobson C Solution conditions determine the relative importance of nucleation and growth processes in alpha-synuclein aggregation. Proc. Natl. Acad. Sci. U.S.A 2014, 111, 7671–7676. [PubMed: 24817693]

(44). Chen MC; Schafer NP; Wolynes PG Surveying the Energy Landscapes of A beta Fibril Polymorphism. J. Phys. Chem. B 2018, 122, 11414–11430. [PubMed: 30215519]

(45). Banerjee S; Hashemi M; Zagorski K; Lyubchenko YL Interaction of Aβ42 with Membranes Triggers the Self-Assembly into Oligomers. Int. J. Mol. Sci 2020, 21, 1129.

(46). Zhao J; Wang Q; Liang G; Zheng J Molecular Dynamics Simulations of Low-Ordered Alzheimer beta-Amyloid Oligomers from Dimer to Hexamer on Self-Assembled Monolayers. Langmuir 2011, 27, 14876–14887. [PubMed: 22077332]

(47). Wälti MA; Ravotti F; Arai H; Glabe CG; Wall JS; Böckmann A; Güntert P; Meier BH; Riek R Atomic-resolution structure of a disease-relevant Aβ(1–42) amyloid fibril. Proc. Natl. Acad. Sci. U.S.A 2016, 113, E4976–E4984. [PubMed: 27469165]

(48). Meng F; Bellaiche MM; Kim J-Y; Zerze GH; Best RB; Chung HS Highly disordered amyloid-β monomer probed by single-molecule FRET and MD simulation. Biophys. J 2018, 114, 870–884. [PubMed: 29490247]

(49). Unpublished results; trajectories. available at http://chemcha-gpu0.ucr.edu/resources/.

(50). Schreiber F Structure and growth of self-assembling monolayers. Prog. Surf. Sci 2000, 65, 151–256.

(51). Cholko T; Kaushik S; Chia-en AC Dynamics and molecular interactions of single-stranded DNA in nucleic acid biosensors with varied surface properties. Phys. Chem. Chem. Phys. 2019, 21, 16367–16380. [PubMed: 31309941]

(52). Roberts CC; Chang C-e. A. Analysis of Ligand-Receptor Association and Intermediate Transfer Rates in Multienzyme Nanostructures with All-Atom Brownian Dynamics Simulations. J. Phys. Chem. B 2016, 120, 8518–8531. [PubMed: 27248669]

(53). Maier JA; Martinez C; Kasavajhala K; Wickstrom L; Hauser KE; Simmerling C ff14SB: improving the accuracy of protein side chain and backbone parameters from ff99SB. J. Chem. Theory Comput 2015, 11, 3696–3713. [PubMed: 26574453]

(54). Jakalian A; Bush BL; Jack DB; Bayly CI Fast, efficient generation of high-quality atomic charges. AM1-BCC model: I. Method. J. Comput. Chem 2000, 21, 132–146.

(55). Northrup SH; Allison SA; McCammon JA Brownian dynamics simulation of diffusion-influenced bimolecular reactions. J. Chem. Phys 1984, 80, 1517–1524.

(56). Berg OG; von Hippel PH Diffusion-controlled macro-molecular interactions. Annu. Rev. Biophys. Biophys. Chem 1985, 14, 131–158. [PubMed: 3890878]

(57). Adam G; Delbrück M Reduction of dimensionality in biological diffusion processes. Struct. Chem. Mol. Biol 1968, 198, 198–215.

(58). Lin Y-C; Petersson EJ; Fakhraai Z Surface effects mediate self-assembly of amyloid-β peptides. ACS Nano 2014, 8, 10178–10186. [PubMed: 25229233]

(59). Pan Y; Banerjee S; Zagorski K; Shlyakhtenko LS; Kolomeisky AB; Lyubchenko YL Molecular Model for the Surface-Catalyzed Protein Self-Assembly. J. Phys. Chem. B 2019, 124, 366–372.

(60). Feig M; Yu I; Wang PH; Nawrocki G; Sugita Y Crowding in Cellular Environments at an Atomistic Level from Computer Simulations. J. Phys. Chem. B 2017, 121, 8009–8025. [PubMed: 28666087]

(61). Piana S; Donchev AG; Robustelli P; Shaw DE Water dispersion interactions strongly influence simulated structural properties of disordered protein states. J. Phys. Chem. B 2015, 119, 5113–5123. [PubMed: 25764013]

(62). Best RB; Zheng W; Mittal J Correction to Balanced Protein-Water interactions improve properties of disordered proteins and non-specific protein association. J. Chem. Theory Comput 2015, 11, 1978. [PubMed: 26574399]

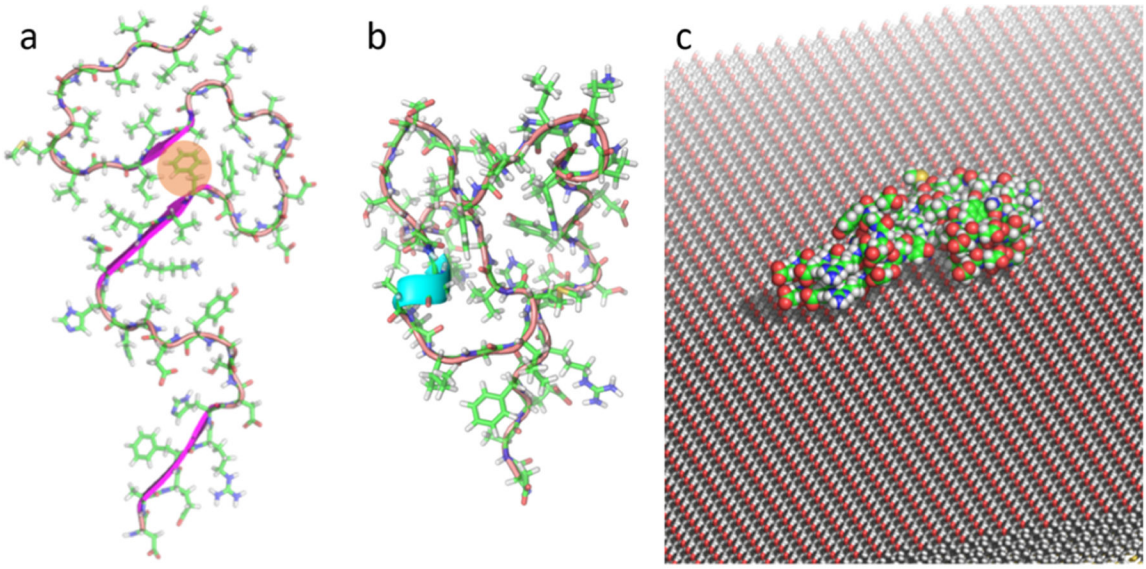

Figure 1.

Structures of the Aβ42 conformations simulated. (a) β-sheet Aβ42 peptide shown in an all-atom representation overlaid with a cartoon representation of the secondary structure (pink and dark pink) to show regions of β-sheet content (dark pink arrows). (b) Random coil Aβ42 conformation shown in the same representation (blue is a small region of α-helix). (c) Aβ42 dimer adsorbed in the middle of the OH-SAM. The adsorbed conformation and position were identical on all other SAMs.

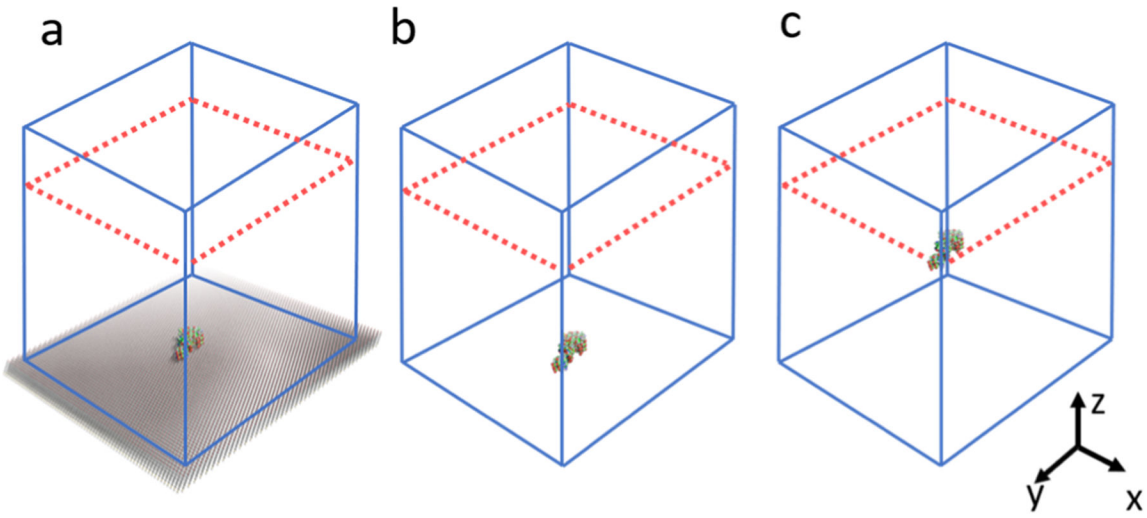

Figure 2.

Depictions of the GeomBD3 simulation space for (a) one of the surface-adsorbed dimer scenarios, (b) no-surface scenario with the dimer positioned at the bottom of the box, and (c) no-surface scenario with the dimer in the center of the box. The dashed red line indicates the starting plane for all Aβ42 monomers and was the same in all simulations.

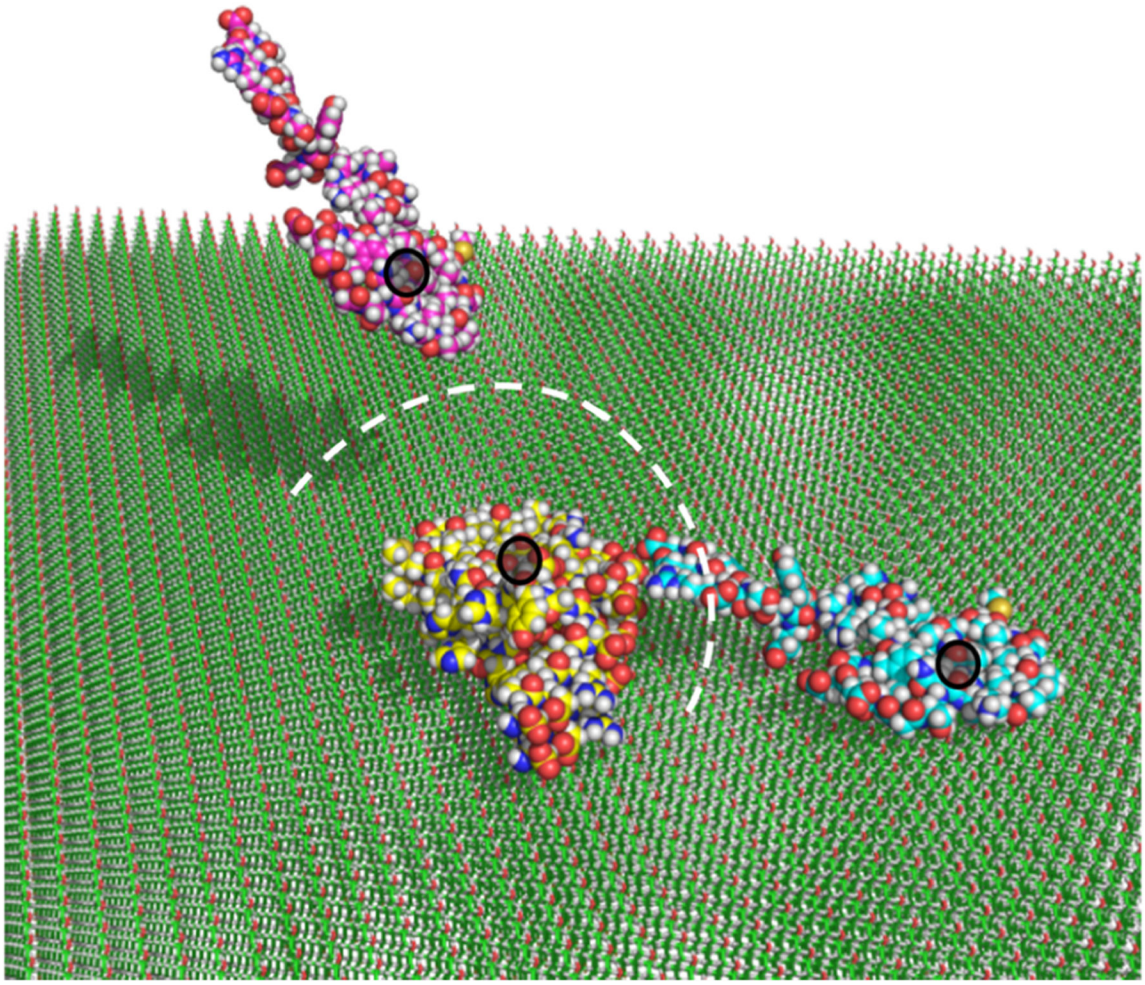

Figure 3.

Example of two-dimensional and three-dimensional association. The association criterion requires residue PHE19 (black circles) of a monomer to be within 40 Å of PHE19 in the dimer (40 Å range approximated by a white dashed line). Here, a surface-adsorbed monomer (blue carbons) approaches the dimer (yellow carbons) and will be considered a two-dimensional associator if the association criterion is satisfied while it is surface-adsorbed. Another monomer (pink carbons) approaches while diffusing in the implicit water solvent and will be a three-dimensional associator if it satisfies the association criterion while freely diffusing three-dimensionally.

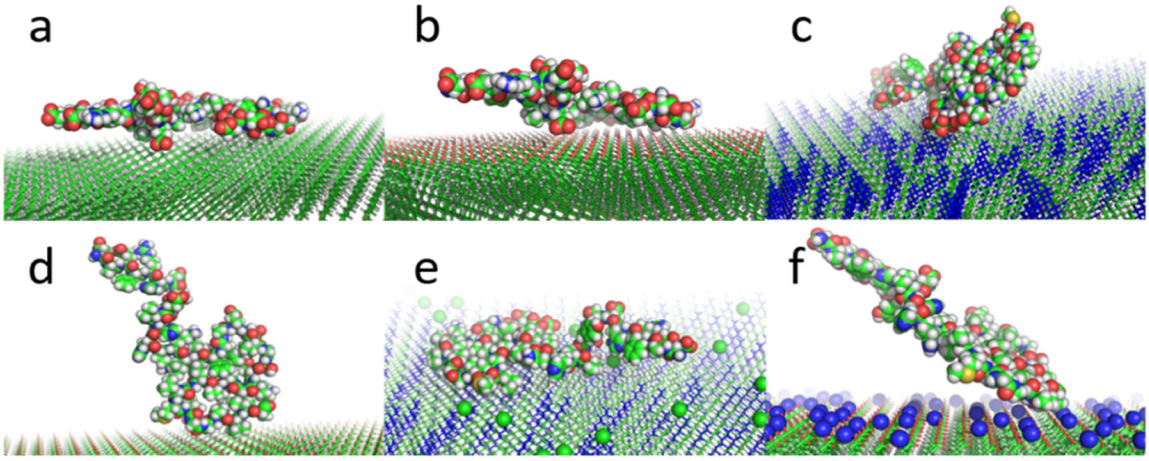

Figure 4.

Adsorption orientations of Aβ42 monomers on the (a) CH_3-SAM, (b) OH-SAM, (c) NH^+-SAM, (d) COO^--SAM, (e) NH^+-SAM(i) (Cl^- ions as green spheres), and (f) COO^--SAM(i) (Na^+ ions as blue spheres). On both NH^+ surfaces, the NH_3^+-containing chains are colored blue to show the inhomogeneous charge distribution, which affects dynamics on the NH^+-SAM more than on the NH^+-SAM(i).

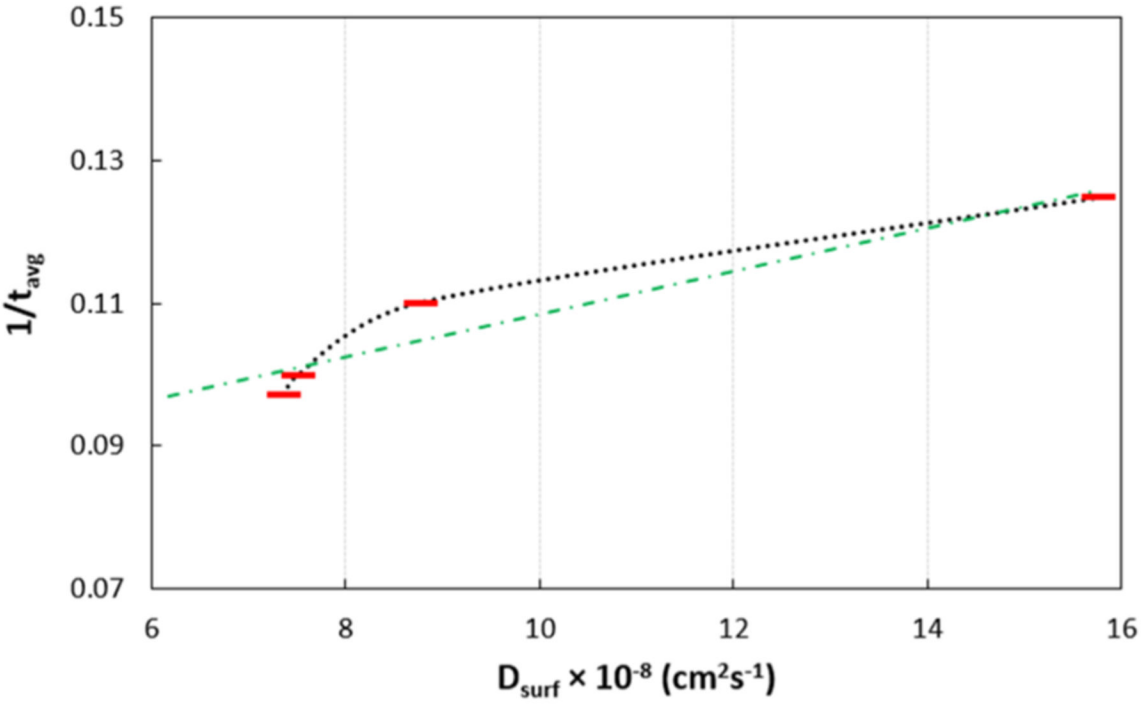

Figure 5.

Plot of inverse average association time versus the surface diffusion coefficient showing the positive trend between the two. These two parameters had the closest direct relationship among the measured pairs. However, the relationship is not perfect since 2D associating monomers must often rotate or reorient to satisfy the association criterion, which can be hindered by inhomogeneous surface affinity of monomers. Additionally, some surface adsorption orientations facilitate association more than others.

Table 1.

Average Association Time (t_{avg}), Monomer-SAM Electrostatic (elec), van der Waals (vdw) Potentials, Ratio of 2D to 3D Associating Monomer Trajectories (2D:3D), Mean Surface Residence Time (t_{res}), and Surface Diffusion Coefficients (D_{surf}) on the Four Different SAMs[a]

Aβ42 monomer surface interactions and association times				
	CH_3-SAM	**OH-SAM**	**NH^+-SAM**	**COO^--SAM**
t_{avg} (μs)	9.08 ± 0.02	10.31 ± 0.05	--	10.01 ± 0.04
E_{elec} (kcal mol^{-1})	−2.3 ± 0.6	0.3 ± 0.8	−38.5 ± 1.7	−18.7 ± 2.7
E_{vdw} (kcal mol^{-1})	−68.3 ± 7.6	−74.1 ± 7.9	−24.0 ± 3.9	−6.0 ± 5.3
2D:3D	8.9	2.7	--	13.5
t_{res} (μs)	7.88	6.82	--	6.35
$D_{surf} \times 10^{-8}$ (cm^2 s^{-1})	8.76 ± 1.66	7.36 ± 1.83	--	7.50 ± 0.73

[a]Some properties (indicated by --) were not measurable or not applicable to specific simulations. Data are mean ± standard deviation (SD). We calculated t_{avg} as a running average, which was updated each time an additional trajectory finished. The SD shown here and in Table 2 is for the last 100 completed trajectories, to demonstrate convergence of the value.

J Phys Chem B. Author manuscript; available in PMC 2021 January 10.

Table 2.

Association Time (t_{avg}), Electrostatic (elec) and van der Waals (vdw) Potentials, Ratio of Two-Dimensionally to Three-Dimensionally Associating Monomer Trajectories (2D:3D), Monomer Surface Residence Time (t_{res}), Monomer Surface Diffusion Coefficients (D_{surf}), and Monomer Bulk Water Diffusion Coefficient (D) on the Ionic SAMs with Adsorbed Counterions (Indicated by (i)) and for the No-Surface Scenarios with the Dimer in the Bottom (bot) or Middle (mid) Position[a]

Aβ42 monomer surface interactions and association times				
	NH^+-SAM(i)	**COO^--SAM(i)**	**no-surface (bot)**	**no-surface (mid)**
t_{avg} (μs)	--	8.01 ± 0.10	6.09 ± 0.09	3.34 ± 0.03
E_{elec} (kcal mol^{-1})	−28.4 ± 3.5	−7.5 ± 6.6	--	--
E_{vdw} (kcal mol^{-1})	−29.6 ± 6.6	−14.5 ± 5.7	--	--
2D:3D	--	4.68	--	--
t_{res} (μs)	--	3.62	--	--
$D_{surf} \times 10^{-8}$ (cm^2 s^{-1})	6.18 ± 1.57	15.6 ± 1.85	--	--
$D \times 10^{-8}$ (cm^2 s^{-1})	--	--	7.95 ± 0.39	7.95 ± 0.39

[a]Some properties (indicated by --) were not measurable or not applicable to specific simulations. Data are mean ± SD.

Table 3.

Comparison of the Average Monomer-Dimer Association Time (t_{avg}) Calculated from Simulation and the Theoretical Average Association Time (t_{theo}) in all of the Different SAM Scenarios and for No-Surface Scenarios with the Dimer in the Bottom (bot) or Middle (mid) Position

theoretical and simulated average association times								
	CH_3-SAM	**OH-SAM**	**NH^+-SAM**	**COO^-SAM**	**NH^+-SAM(i)**	**COO^--SAM(i)**	**bot**	**mid**
t_{avg} (μs)	9.08	10.31		10.01		8.01	6.09	3.34
t_{theo} (μs)	20.7	22.1		23.8		13.6	8.26	8.26
t_{theo}/t_{avg} (μs)	2.28	2.14		2.38		1.67	1.36	2.47

J Phys Chem B. Author manuscript; available in PMC 2021 January 10.